Electronic Supplementary Material (ESI) for Journal of Materials Chemistry B.

Supplementary Information

Multifunctional theragnostic ultrasmall gold nanodots-encapsuled perfluorocarbon nanodroplets for laser-focused ultrasound sequence irradiation (LFSI)-based enhanced tumor ablation

Menghan Xu,[a] Wei Long,[a] Xiang Ling,[a] Xiongwei Hu,[a] Hao Hong,[b] Yayun Peng,*[a] and Ting Cai*[a]

[a]State Key Laboratory of Natural Medicines, Department of Pharmaceutics, China Pharmaceutical University, Nanjing 210009, China

[b]State Key Laboratory of Pharmaceutical Biotechnology, Jiangsu Key Laboratory of Molecular Medicine and School of Medicine, Medical School of Nanjing University, Nanjing 210093, China

* Corresponding authors:

E-mail: yypeng@cpu.edu.cn (Yayun Peng)

E-mail: tcai@cpu.edu.cn (Ting Cai)

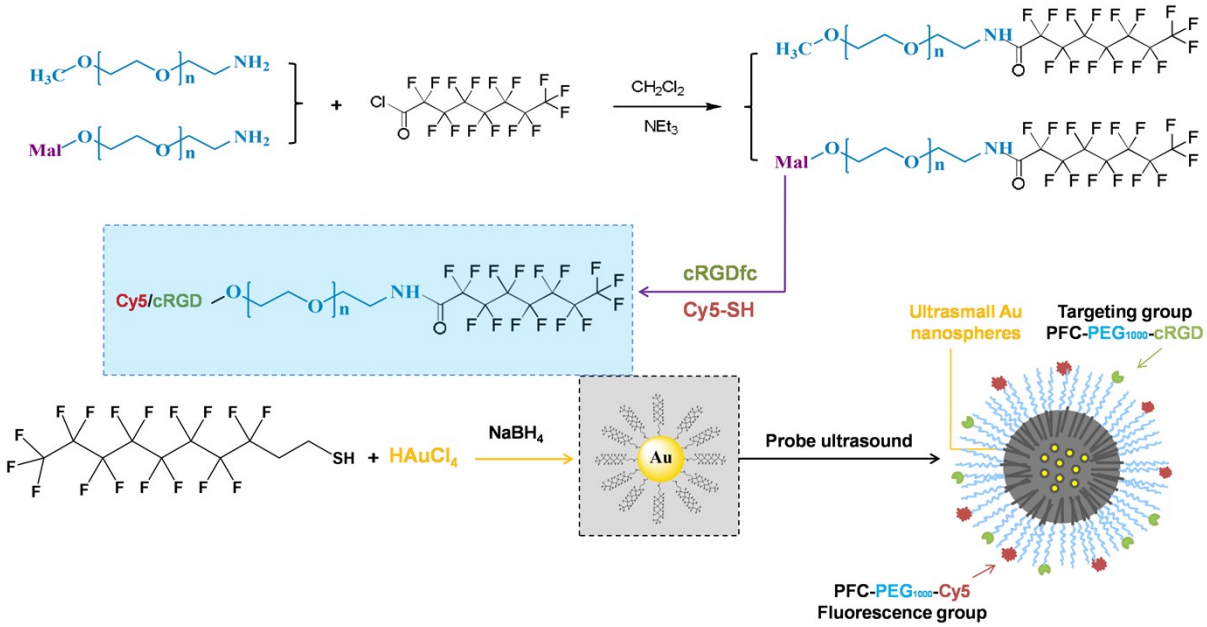

Fig. S1. Schematic illustration of the synthetic route of PFC-PEG$_{1000}$, PFC-PEG$_{1000}$-cRGD/Cy5, and Au nanodots and the preparation of Au-PFCnDs and Cy5/cRGD-modified Au-PFCnDs.

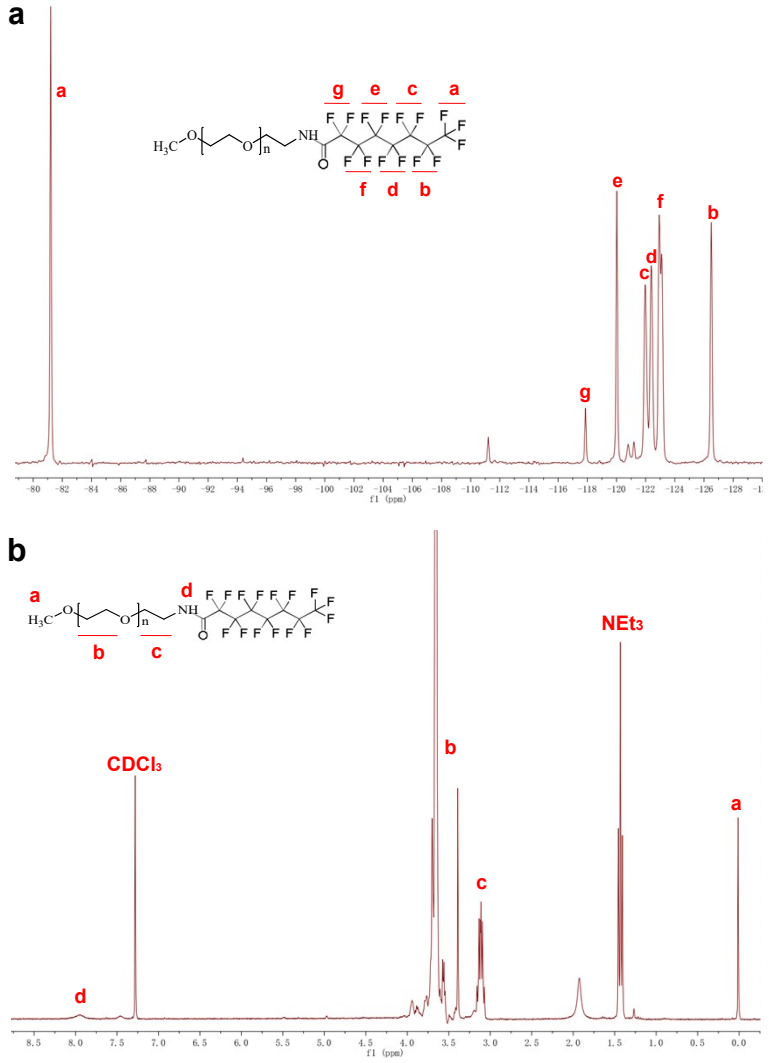

Fig. S2. ^{1}H NMR and ^{19}F NMR spectra of PFC-PEG_{1000}

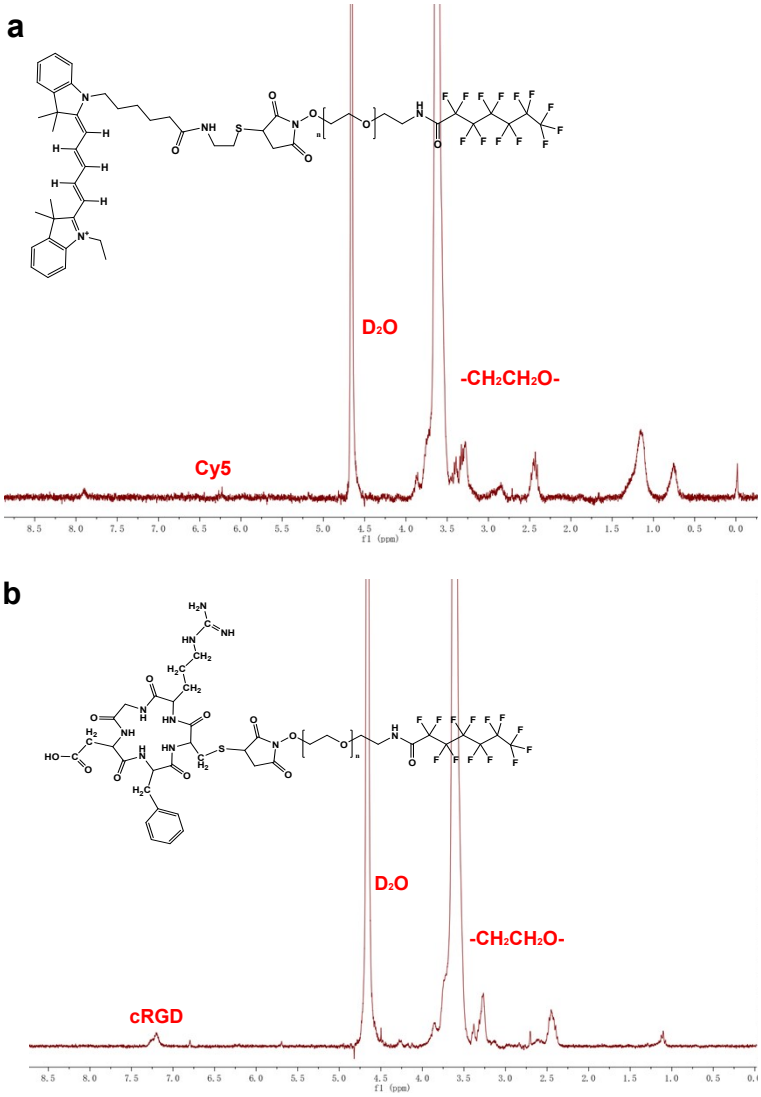

Fig. S3. ^{1}H NMR spectra of PFC-PEG_{1000}-cRGD/Cy5

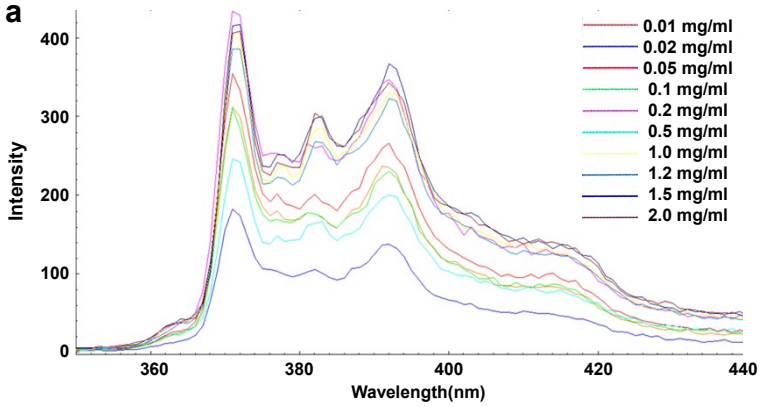

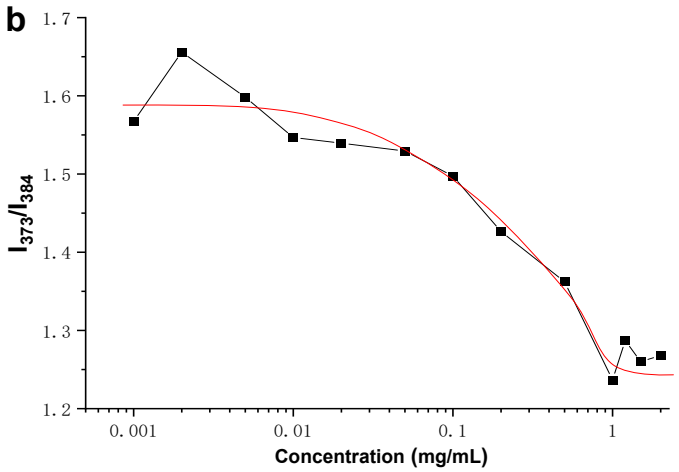

Fig. S4. (a) Fluorescence spectra (Ex = 335 nm) of pyrene (6.0×10^7 M) in water in the presence of increasing concentrations of PFC-PEG_{1000}. (b) Plots of the ratio of intensities (I_{373}/I_{384}) of the vibrational bands in the pyrene fluorescence spectra as a function of polymer concentration in the CMC test.

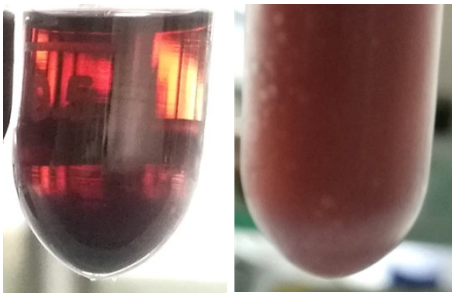

Fig. S5. Homogeneous dispersion of Au nanodots in perfluorohexane (PFH) and prepared Au-PFCnDs dispersed in water.

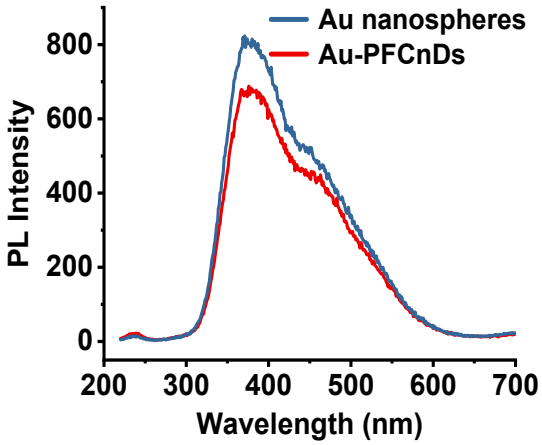

Fig. S6. Fluorescence spectra of Au nanodots in perfluorohexane (PFH) and prepared Au-PFCnDs dispersed in water.

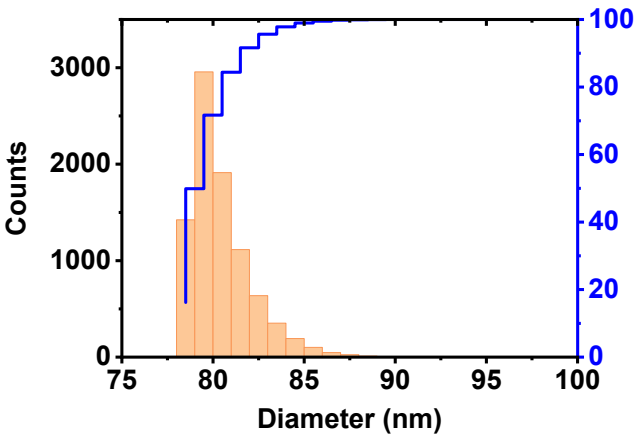

Fig. S7. Particle size distribution of Au-PFCnDs dispersed in water (TEM).

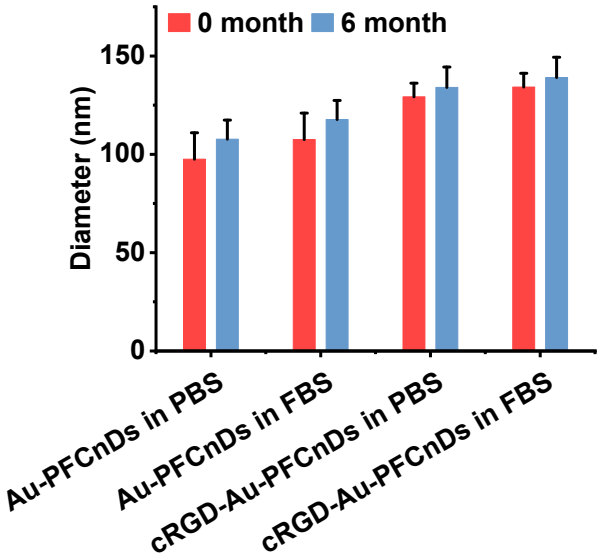

Fig. S8. Particle size change of Au-PFCnDs dispersed in water after storage at 4 °C for more than half a year.

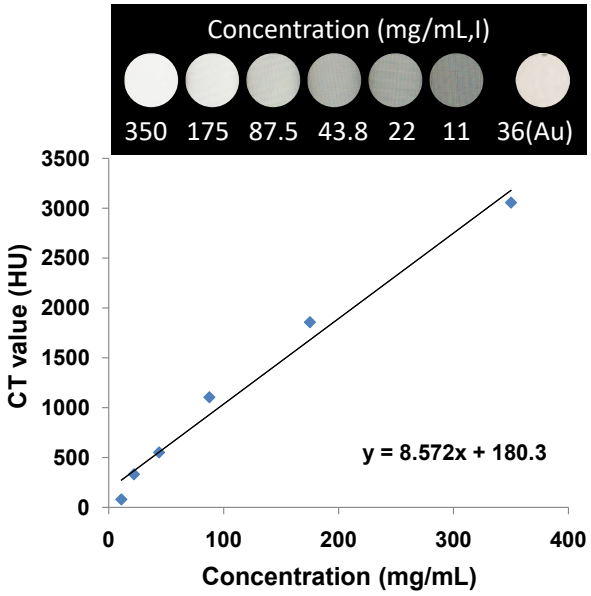

Fig. S9. CT value of iohexol aqueous solutions versus the concentration of I.

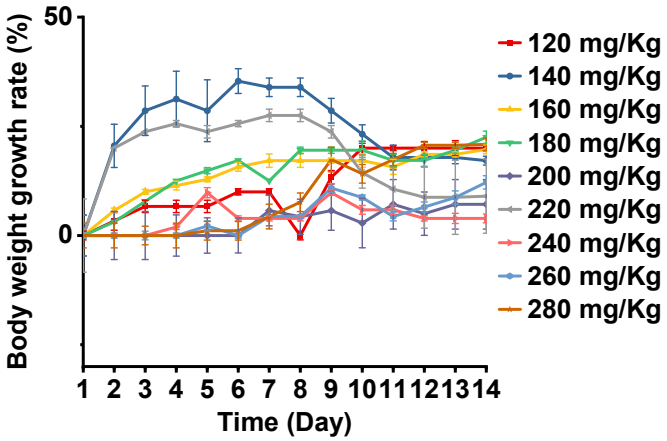

Fig. S10. Body weight change curve of healthy mice after tail vein injection at different doses

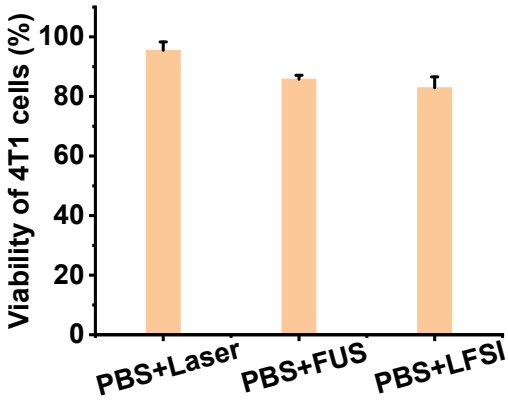

Fig. S11. The viability of 4T1 cells incubation with PBS for 24 h after laser, FUS, and LFSI treatment 20 s

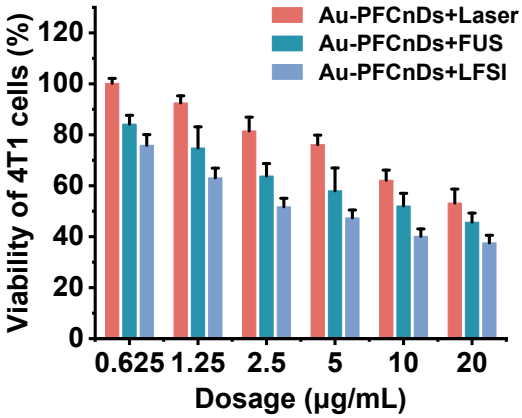

Fig. S12. The viability of 4T1 cells after treatment with various concentrations of Au-PFCnDs under the laser, FUS, and LFSI treatment.

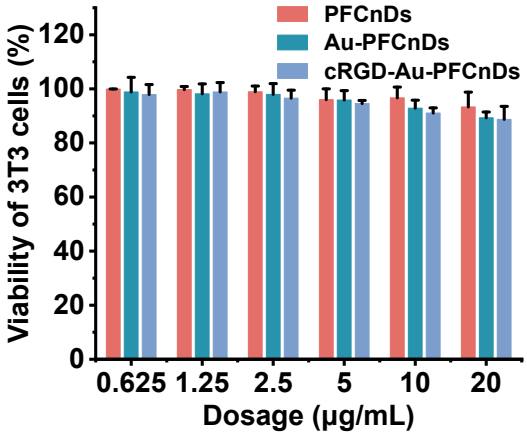

Fig. S13. The viability of 3T3 cells incubation with different concentrations of PFCnDs, Au-PFCnDs, and cRGD-Au-PFCnDs for 24 h

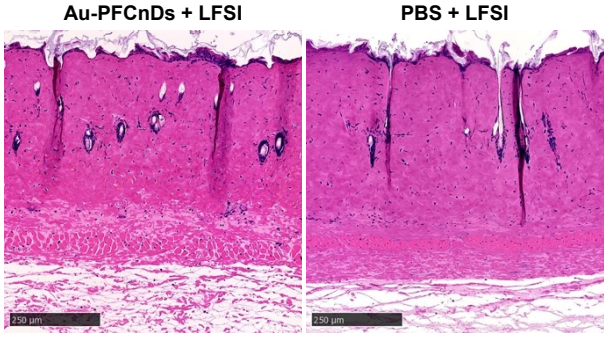

Fig. S14. Mouse skin pathology sections after Au-PFCnD-mediated LFSI treatment (H&E staining)

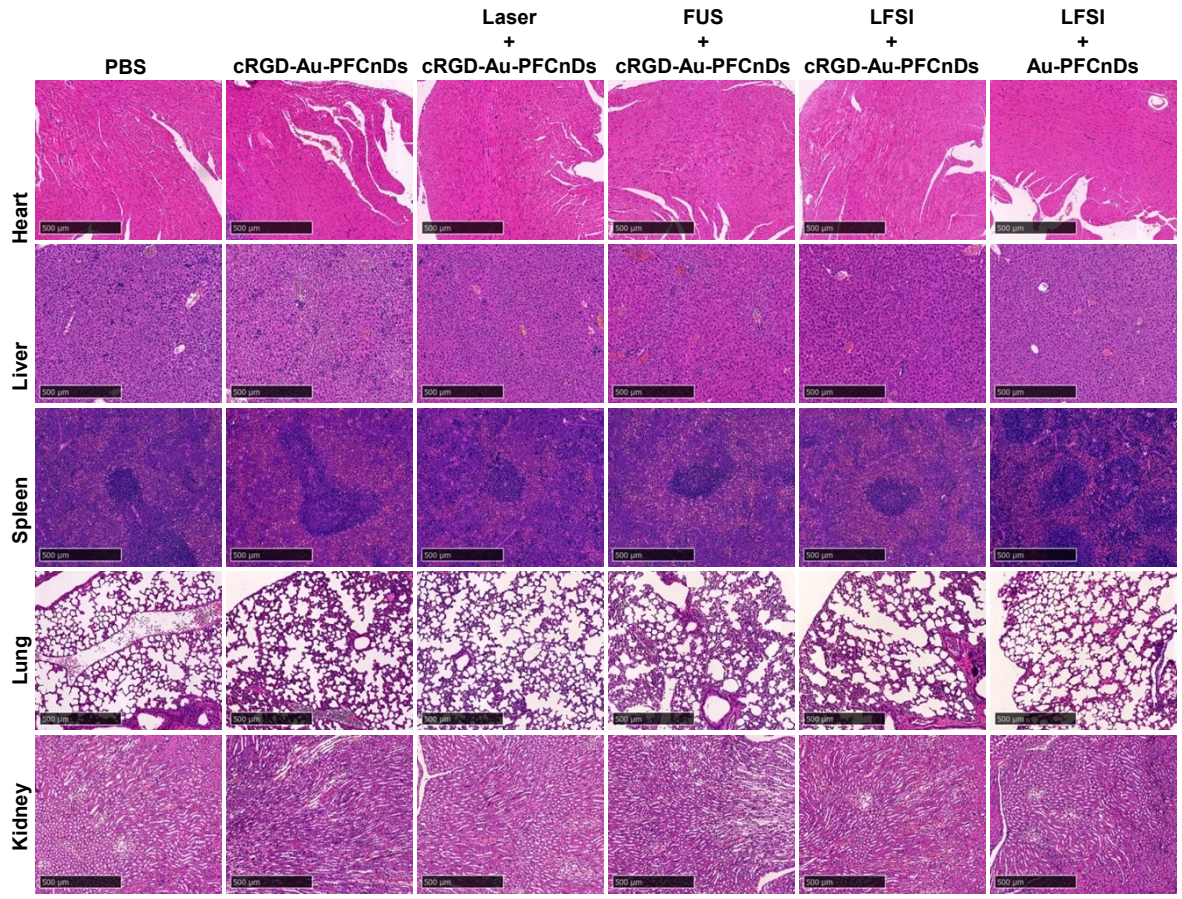

Fig. S15. H&E assay of the main organs (heart, liver, spleen, lung, kidney) after treatments of the 4T1 tumor-bearing mice (n=5).

Table S1. Blood biochemistry and routine examination (n=3)

		PBS	cRGD-Au-PFCnDs	Laser + cRGD-Au-PFCnDs	FUS + cRGD-Au-PFCnDs	LFSI + cRGD-Au-PFCnDs	LFSI + cRGD-Au-PFCnDs
AST	U/L	271.7 ± 9.3	257.7 ± 38.8	220.3 ± 43.9	203.0 ± 15.7	208.0 ± 8.5	220.0 ± 37.8
ALT	U/L	38.7 ± 2.2	39.0 ± 0.6	38.0 ± 3.8	35.3 ± 0.7	37.7 ± 3.0	48.7 ± 0.7
ALP	U/L	54.3 ± 8.3	57.3 ± 2.4	55.7 ± 9.7	58.7 ± 4.4	58.0 ± 4.6	87.3 ± 16.8
BUN	mm/L	9.3 ± 2.3	7.4 ± 1.0	6.9 ± 1.0	7.1 ± 0.6	5.4 ± 0.5	6.4 ± 0.6
CREA	um/L	5.5 ± 2.7	5.2 ± 2.4	10.5 ± 1.4	6.0 ± 1.4	9.7 ± 2.4	9.9 ± 3.4
HGB	g/dl	13.0 ± 0.4	11.6 ± 0.8	10.7 ± 1.1	23.2 ± 12.7	12.2 ± 0.4	9.5 ± 4.4
WBC	10*9 cell/L	262.9 ± 9.3	383.2 ± 28.4	136.1 ± 66.0	220.4 ± 26.4	92.9 ± 40.8	108.8 ± 101.0
RBC	10*12 cell/L	8.2 ± 0.2	7.3 ± 0.5	6.8 ± 0.8	9.7 ± 2.6	8.1 ± 0.2	6.4 ± 2.9
PLT	10*9 cell/L	695.0 ± 69.8	741.0 ± 77.9	372.7 ± 170.3	675.0 ± 11.3	206.0 ± 46.0	426.3 ± 194.8
Retic	%	5.9 ± 0.6	3.8 ± 0.5	5.9 ± 2.1	4.6 ± 0.2	3.2 ± 0.2	3.9 ± 0.8
Neut	%	94.9 ± 0.2	96.0 ± 0.3	89.7 ± 4.7	93.4 ± 1.5	87.2 ± 3.8	66.5 ± 20.9
Lymph	%	3.5 ± 0.2	2.6 ± 0.2	6.9 ± 3.9	4.9 ± 1.6	8.4 ± 3.9	26.6 ± 18.3